



# Design Considerations of a Dual Mode X-Band EPR Resonator for Rapid In-Situ Microwave Heating

Michael Barter<sup>1</sup> · Giuseppina Magri<sup>2</sup> · Jaafar Harari<sup>1</sup> · Heungjae Choi<sup>1</sup> · Andrea Folli<sup>2</sup> · Daniel R. Slocombe<sup>1</sup> · Emma Richards<sup>2</sup> · Damien M. Murphy<sup>2</sup> · Adrian Porch<sup>1</sup>

Received: 1 November 2021 / Revised: 10 December 2021 / Accepted: 14 January 2022  
© The Author(s) 2022

## Abstract

This paper describes the design considerations for a dual mode X-band continuous wave (CW) Electron Paramagnetic Resonance (EPR) cavity, for simultaneous EPR measurement and microwave heating of the same sample. An elliptical cavity geometry is chosen to split the degeneracy of the  $TM_{110}$  mode, allowing for a well resolved EPR signal with the  $TM_{110,a}$  and  $TM_{110,b}$  modes resonating at around 10 GHz and 9.5 GHz, respectively, the latter of which is used for EPR measurements. This geometry has the benefit that the  $TM_{010}$  mode used for microwave heating resonates at 6.1 GHz, below the cut off frequency of the X-band waveguide used for the EPR channel, providing effective isolation between the heating and EPR channels. The use of a pair of 9  $\mu\text{m}$  thick copper clad laminates as the flat cavity walls allows for sufficient penetration of the modulation field ( $B_{\text{mod}}$ ) into the cavity, as well as maintaining a high cavity Q factor ( $> 5700$ ) for sensitive EPR measurements. Locating the heating port at an angle of  $135^\circ$  to the EPR port provides additional space for easier coupling adjustment and for larger sample access to be accommodated. The associated decrease of EPR signal strength is fully compensated for by using a 7.2 GHz low pass filter on the heating port. EPR spectra using 1.6 mm and 4.0 mm sample tubes are shown at room temperature (298 K) and 318 K for a standard  $\text{Cu}(\text{acac})_2$  solution, demonstrating the effectiveness of this dual-mode EPR cavity for microwave heating during EPR detection.

---

✉ Michael Barter  
BarterM@cf.ac.uk

<sup>1</sup> Centre for High Frequency Engineering, School of Engineering, Cardiff University, Cardiff CF24 3AA, UK

<sup>2</sup> School of Chemistry, Cardiff University, Main Building, Park Place, Cardiff CF10 3AT, UK

## 1 Introduction

The Zeeman splitting of electronic spin states via an applied DC magnetic field is essential for detecting Electron Paramagnetic Resonance (EPR) spectra of paramagnetic substances [1]. The interactions between an unpaired electron with neighboring magnetic nuclei and/or other unpaired electrons impart spectral features from which information on molecular structure, bonding, dynamics in solution, concentration and reactivity can be ascertained [2–5]. EPR plays a major role in investigating industrially relevant catalytic reactions involving paramagnetic species and free radicals [6–9]. The motivation to develop a dual mode resonator was driven by our need to better understand the mechanism of catalytic reactions, particularly those enhanced by microwaves. It is well known that microwaves can be used to accelerate and drive chemical reactions, and that effective energy transfer is accomplished using resonant microwave applicators [10–13]. Furthermore, rapid heating can change not only the selectivity and product distribution of some reactions, but also provides a simple and effective means to study the dynamics and possible speciation of the reacting system itself, for example, via the application of a rapid temperature-jump (TJ) [14–16]. With this in mind, we recently introduced the concept of a dual mode “reactor-resonator” EPR cavity [17] that doubles up as an effective applicator for heating a sample but also allows for simultaneous EPR spectroscopy to be performed, simply by selection of two distinct resonant modes of different resonant frequencies.

At the heart of most EPR spectrometers is a microwave cavity, with microwaves at the cavity’s resonant frequency used to provide the necessary energy to excite unpaired electrons between different spin energy levels [18–21]. EPR coupling is to the microwave’s magnetic field  $B_1$ , in which the sample under investigation must reside, which is usually applied perpendicular to the DC magnetic field  $B_0$ . In continuous wave (CW) EPR, the EPR spectrum is generated by AC modulation of  $B_0$  by a small amplitude  $B_{\text{mod}}$  (typically at 100 kHz) via a pair of separate modulation coils, which gives rise to a modulation (also at 100 kHz) of the microwave power absorbed at the resonant (EPR) frequency. This is measured directly by the resulting modulation in the reflected power of the EPR cavity when critically coupled and tuned to the EPR frequency, so that the EPR signal is proportional to the cavity’s quality factor  $Q$  and the effective volume filling factor (i.e., the sample volume divided by the effective cavity volume). The EPR spectrum is generated by measuring the modulated reflected power as the applied DC field  $B_0$  is swept. In this work, we restrict our discussion to CW (as opposed to pulse) X-band microwave frequencies (around 9.5 GHz) as most commonly used for EPR measurements, though EPR spectrometers are commercially available at other frequencies, including for example Q-band (35 GHz) and W-band (95 GHz), amongst others.

This paper, therefore, describes in detail some of the general design features that are necessary for the dual mode cavity to operate effectively, focusing on three main requirements: (a) to preserve a high quality factor  $Q$  for the EPR mode, which is necessary for a high signal to noise ratio of the resulting EPR

signal; (b) to ensure the effective exposure of the sample to the modulation field  $B_{\text{mod}}$ , which is necessary to allow phase sensitive detection to amplify the EPR signal and convert the signal from an absorbance profile to its first harmonic; and (c) to remove interference between the heating “channel”, which involves high-power microwaves (of a few W) at a frequency of around 6.1 GHz, with the sensing (EPR) “channel”, involving low power microwaves (of a few mW) around 9.5 GHz.

## 2 Resonator Design Considerations

The central premise for our dual mode reactor–resonator is to use the lower frequency cavity mode for heating the sample under investigation, in which the sample itself is located in the microwave electric field, while the higher frequency mode is used for EPR measurement, in which the sample is located in the magnetic field. The choice of frequency for the heating component of the dual mode resonator is determined by the bandwidth of the rectangular X-band waveguide used to couple to the EPR mode in most commercial CW EPR systems. This has a lower cutoff frequency of 6.5 GHz for its  $TE_{01}$  mode, taking the long waveguide dimension of 22.9 mm; hence it will act as an almost perfect high pass filter, reflecting the high-power microwaves used to excite the heating mode, provided these are substantially below 6.5 GHz. Assuming 6.1 GHz for the heating mode and 9.7 GHz for the EPR mode, the 1.0:1.6 frequency ratio required can be met with a near square or cylindrical cavity resonator design. At 6.1 GHz, the X-band rectangular waveguide has an attenuation coefficient of around 4.3 dB/cm, so the 50 cm (or longer) section of the X-band waveguide, used to mount the cavity into the space between the magnet pole pieces, will give at least 200 dB of attenuation.

We use a cylindrical aluminium cavity resonator (of nominal internal diameter of 19 mm) designed to operate simultaneously in its 6.1 GHz  $TM_{010}$  mode (for heating) and 9.7 GHz  $TM_{110}$  mode (for EPR). The electric and magnetic field energies on the cavity cross section of the relevant modes are presented in Fig. 1. The cavity is oriented so that its axis is perpendicular to the applied DC magnetic field  $B_0$ . The microwave electric field distribution of the  $TM_{010}$  mode has a maximum along the whole internal length of the cavity’s axis; the sample is introduced into this high electric field region. However, the  $TM_{110}$  EPR mode is doubly degenerate, having two orthogonal modes. To split this degeneracy, we adopt an elliptical cross section of semi-major and minor axes of  $a = 19.7$  mm and  $b = 17.8$  mm, respectively. This leaves the  $TM_{010}$  frequency approximately unaltered at  $f_{010} \approx 6.1$  GHz, but the  $TM_{110}$  degeneracy is split to  $f_{110,a} \approx 10$  GHz, and  $f_{110,b} \approx 9.5$  GHz; the latter of these is used for the EPR measurement and the 500 MHz splitting is found to be sufficient to obtain excellent quality EPR spectra. Using COMSOL Multiphysics simulations, we also find that the elliptical geometry provides greater separation of the magnetic and electric fields near the cavity axis, which is important for maintaining a high  $Q$  factor for samples which have a high microwave loss, such as samples containing very polar solvents.

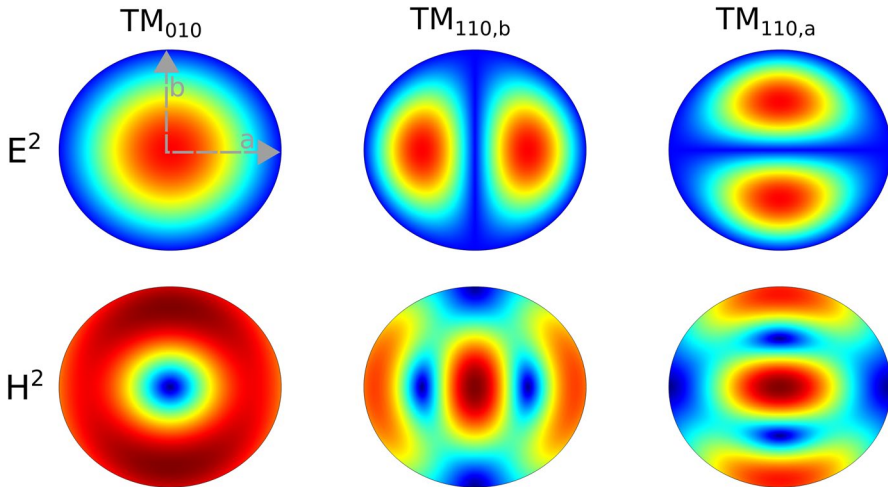


**Fig. 1** Microwave electric and magnetic energy densities ( $E^2$  and  $H^2$ , respectively) of the dual-mode elliptical cavity. The  $E$  fields are perpendicular to the page, whereas the  $H$  fields are in the plane of the page

Although the height of the cavity is not a factor for the calculation of the TM resonant frequencies of both the heating and EPR modes, we have carefully chosen it to have an internal dimension of 15 mm; this is large enough to ensure a high enough  $Q$  factor for the empty cavity in the EPR and heating modes (both over 5000), but short enough to prevent interference with the  $TE_{111}$  mode (kept at above 11 GHz), and to maintain uniformity across the sample length of the modulation field  $B_{\text{mod}}$ . Since we only use the  $TM_{110,b}$  mode for EPR, from this point onwards we will refer to this mode as  $TM_{110}$  for simplicity.

Constructed and exploded render views of the cavity are shown in Fig. 2a, and b, respectively. The main body of the elliptical cylinder is CNC machined from aluminium due to its high electrical conductivity, ease of machining, and low cost. It is important for the flat walls of the cavity to be prepared with minimum thickness to allow penetration of the modulation field  $B_{\text{mod}}$  into the cavity, generated by a pair of Helmholtz modulation coils with their axis aligned with the axis of the cavity. This is achieved by implementing single-coated Rogers Corporation RT/Duroid 5880 copper laminates, which provide a thin copper layer with a supporting glass microfiber reinforced PTFE layer. The copper layers make direct contact with the aluminium body and have very high electrical conductivity, which, therefore, results in an increase of the cavity  $Q$  factor.

To select the optimum copper layer thickness, the 100 kHz modulation field  $B_{\text{mod}}$  distribution was simulated using COMSOL Multiphysics for laminates of copper thickness 9, 18 and 35  $\mu\text{m}$ , as shown in Fig. 3 as a function of position along the cavity's axis; these were the laminates used in the experiments. Assuming the electrical conductivity of copper to be  $5.6 \times 10^7$  S/m, the skin depth in copper at the modulation frequency of 100 kHz is approximately 210  $\mu\text{m}$ . The reduction of  $B_{\text{mod}}$  at the sample position (i.e., 0 mm on the  $x$ -axis of Fig. 3) and

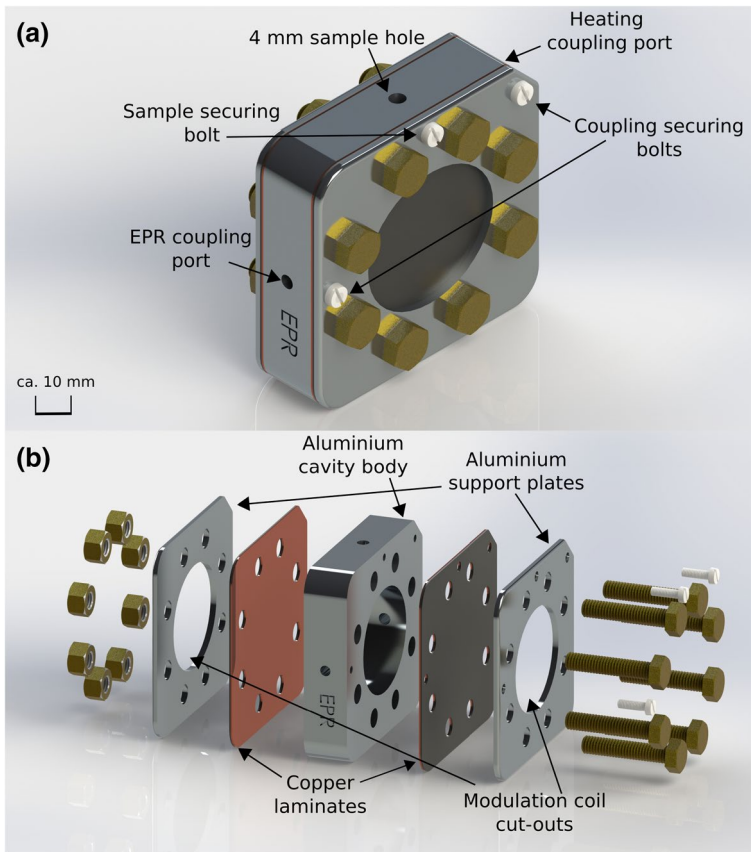


**Fig. 2** Render of cavity design in **a** fully constructed, and **b** exploded views

the redistribution of  $B_{\text{mod}}$ , both due to the screening of the copper plates, are evident in Fig. 3. However, we note that the pair of  $9 \mu\text{m}$  thick copper laminates only reduce  $B_{\text{mod}}$  by around 52% within the cavity and so we implement a pair of  $9 \mu\text{m}$  thick copper laminates for the flat cavity surfaces. We ensure that they are firmly bolted (using non-magnetic brass M6 nuts and bolts) to the aluminium block containing the elliptical cavity space, since the mechanical joint between them carries a microwave current.

To confirm the COMSOL simulations of Fig. 3, we have studied the effects of the copper laminate thickness on  $B_{\text{mod}}$  and  $Q$  experimentally. In Fig. 4a we show the magnetic field at the sample space generated by the 70 turn, 14 mm radius modulation coils, with a  $5 V_{\text{pp}}$ , 100 kHz signal. Magnetic field was calculated as a function of the copper laminate thickness, measured experimentally via the pick-up voltage of a 2 mm radius circular search coil with 200 turns inserted into the cavity and fixed at the sample position. Rogers Corporation RT/Duroid 5880 copper laminates of thickness 9, 18 and  $35 \mu\text{m}$  are used here; these measurements

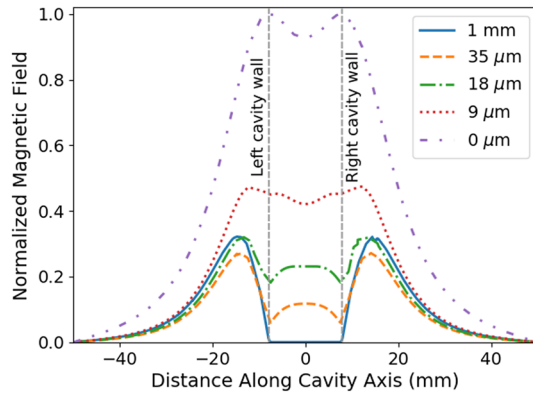


**Fig. 3** COMSOL Multiphysics simulation of amplitude of the 100 kHz modulation magnetic field along the central cavity axis (sample located at 0 mm). The cavity's flat walls are positioned at axial positions of  $\pm 7.5$  mm; with the modulation coils positioned at  $\pm 9.5$  to 11.5 mm. Each plot corresponds to pairs of copper laminates used for the flat cavity walls, of thicknesses 9, 18 and 35  $\mu\text{m}$ . Also shown are the effects of a pair of 1 mm thick copper plates, which effectively extinguish the modulation field in the cavity space. The effect of no cavity walls is also shown (0  $\mu\text{m}$ )

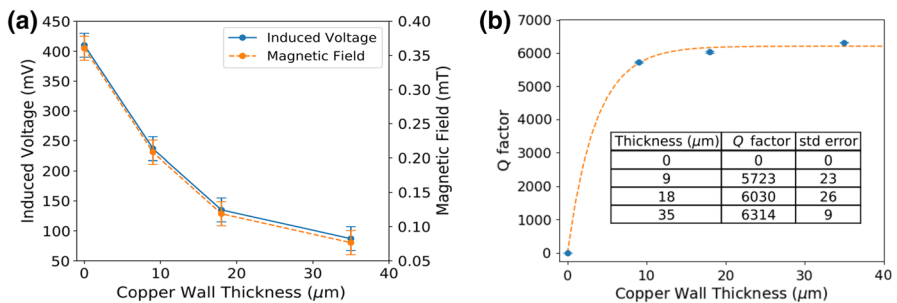


**Fig. 4** Graphs showing the experimentally determined **a** 100 kHz modulation field inside the cavity (i.e., the experimentally measured pick-up voltage on a search coil at the center of the cavity, and the calculated modulation field based on the known current through the Helmholtz modulation coils) where noise floor voltage measurement is 20 mV determining the error bars, and **b** the  $Q$  factor for the  $\text{TM}_{110}$  mode of an empty cavity, both as a function of the copper laminate (i.e., wall) thickness. The standard error bars (from three measurement repeats) are shown but are too small to show effectively in these graphs and so are also listed in the tables in the insets

confirm that, as expected, the minimum disruption to  $B_{\text{mod}}$  is when using the thinnest (i.e., 9  $\mu\text{m}$ ) copper thickness.

One of the potential drawbacks of using thin copper plates for the cavity's flat surfaces is the associated reduction in  $Q$ , which is most important for the  $\text{TM}_{110}$  EPR mode. For a cylindrical cavity, to which our elliptical cavity is a good approximation, the conductor quality factor for any  $\text{TM}_{mn0}$  mode is given as

$$\frac{1}{Q_{m0}} = \frac{\delta_{\text{curv}}}{a} + \frac{\delta_{\text{flat}}}{d}, \quad (1)$$

where  $\delta$  is the microwave skin depth in the curved and flat wall portions of the cavity,  $a$  is the inner radius and  $d$  the inner length. This assumes that all metal thicknesses are much greater than the skin depth. Taking  $a=19$  mm,  $d=15$  mm and assuming electrical conductivities of  $5.6 \times 10^7$  S/m and  $3.6 \times 10^7$  S/m for copper (flat surfaces) and aluminium (curved surface), respectively, gives skin depths at 9.5 GHz of  $0.69 \mu\text{m}$  and  $0.86 \mu\text{m}$  for the flat and curved surfaces, respectively; this gives a “theoretical” value of  $Q_{110}$  to be approximately 10,900. In practice, measured conductor  $Q$  factors are typically 25–30% less than theoretical values owing to surface roughness effects (which increases the effective surface area) and degraded electrical quality of the surface of a metal (due to surface strain, for example).

The measured  $Q_{110}$  data for the empty composite Cu/Al elliptical cavity of our standard design shown in Fig. 4b were obtained via measurements of voltage transmission coefficient  $S_{21}$  using a Keysight E5071C vector network analyzer, again with the flat copper surfaces made up from Rogers Corporation RT/Duroid 5880 laminates of copper thickness varying between  $9 \mu\text{m}$ ,  $18 \mu\text{m}$  and  $35 \mu\text{m}$ . The error bars represent standard errors from three repeats of the same measurement, reconstructing the cavity with the different laminates each time. The results illustrate a 9.4% decrease in  $Q_{110}$  when decreasing the copper thickness from 35 to  $9 \mu\text{m}$ , from  $6314 \pm 9$  to  $5723 \pm 23$ . We would expect  $Q_{110}$  to be no greater than 8000 when using flat plates of similar grade copper of a few mm thickness (which is not obtainable in circuit board form) so the compromised choice of  $9 \mu\text{m}$  thick copper laminates allows a high enough  $Q$  factor ( $5723 \pm 23$ ) for sensitive EPR measurements, while not reducing significantly the modulation field  $B_{\text{mod}}$  at the sample position through screening at 100 kHz (from the data of Figs. 3 and 4b); hence we proceeded to construct the cavity with this thickness of copper laminates.

Returning to the constructional details as presented in Fig. 2, a 4 mm sample hole is drilled through the cavity to allow for sample access, using a standard EPR sampling tube. Both  $\text{TM}_{010}$  (heating) and  $\text{TM}_{110}$  (EPR) modes are magnetically coupled to external circuits using loop-terminated RG402 coaxial cable. A flexible coaxial cable is used to connect to the X-band waveguide of the EPR system via a coax to waveguide adaptor. Additional holes are also included in the cavity body for attachment and mechanical adjustment of these coupling loops, since both need to be adjusted to achieve critical coupling for both modes of operation. Non-magnetic nylon bolts are used to secure coupling structures and the sample in place. An observation hole is also included on the opposite side to the EPR port to allow sample temperature measurements using an external thermal camera. Accurately determining the temperature of a sample heated via microwaves is challenging and alternative methods of determining temperature are being explored.

The 6.1 GHz microwave heating system is described in detail in [17], but briefly comprises a low-power, solid state source (Keysight N5173B) with a power amplifier (Empower 1131—BBM5K8CGM) of saturated output power of 35 W and 10 W at 1 dB compression point. This amplifier is connected to the cavity heating port via a flexible coaxial cable. We find this is capable of generating heating rates of 10 K/s

when using commonly used organic solvents, which is more than sufficient for the needs of our catalytic investigations.

### 3 EPR Measurement Details

In our first-generation dual-mode cavity [17], we adopted the coupling scheme shown in Fig. 5a, where the coupling loop for the heating port was positioned at a null of the microwave magnetic field of the EPR mode. In this configuration, the coupling loop of the heating mode is naturally isolated from the magnetic field of the EPR mode, meaning that it has no loading effect on the EPR  $Q$  factor. However, because of this relative placement of the two coupling ports, a sample size limitation is inherently introduced, restricting the sample tube diameter to only 1.6 mm with subsequent limitations on sample volume for EPR analysis. Therefore, in our second-generation cavity presented in this work, to accommodate a larger 4 mm diameter sample tube (and thus greater sampling volume) and to allow easier coupling adjustments to be made, the heating port was reconfigured and re-positioned at an angle of  $135^\circ$  relative to the EPR port. In this orientation, the heating port is still located in a region of low magnetic field but is no longer positioned at the null, as illustrated in Fig. 5b. While sample volume can be increased due to this new orientation, it is important to consider the resulting impact on the EPR  $Q$  factor and potential loss of sensitivity in the resulting EPR spectrum.

The resulting EPR spectra recorded using our new composite cavity design at both 298 K and 318 K (utilizing simultaneous EPR detection and 6.1 GHz heating) are shown in Fig. 6, based on a standard 20 mM  $\text{Cu}(\text{acac})_2$  (copper (II) acetylacetonate) solution (in  $\text{CHCl}_3$  solvent), to directly compare the current results to those obtained using our first-generation dual-mode cavity [17]. A 100  $\mu\text{l}$  aliquot of this standard solution was loaded into a 1.6 mm  $Q$ -band EPR tube (product number: WG-221 T-RB Wilmad Labglass, O.D=1.6 mm and I.D=1.1 mm), to a sample depth of 90 mm to maximise the cavity filling factor.

It is immediately clear that the 298 K and 318 K recorded EPR spectra for  $\text{Cu}(\text{acac})_2$  (Fig. 6a, b) suffer noticeably from high noise and (in this initial cavity

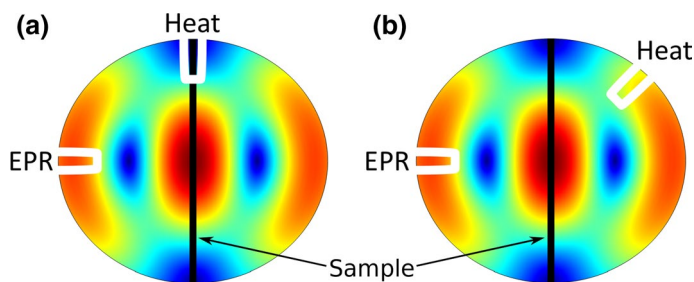


**Fig. 5** Microwave magnetic field magnitudes of the  $\text{TM}_{110}$  mode indicating heating and EPR port placement in our **a** first-generation [17], and **b** the second-generation dual-mode cavity design used in this work



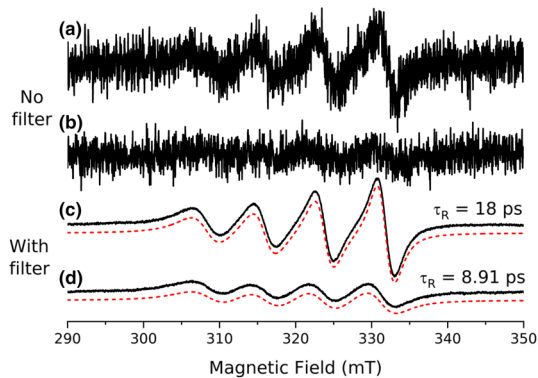


**Fig. 6** X-band CW-EPR spectra of 20 mM  $\text{Cu}(\text{acac})_2$  solution in  $\text{CHCl}_3$  recorded in a 1.6 mm EPR tube at **a** 298 K (without filter), **b** 318 K (without filter), **c** 298 K (with filter), and **d** 318 K (with filter). All spectra were acquired on the second-generation composite Cu/Al dual-mode cavity, employing 100 kHz field modulation, 0.1 mT modulation depth,  $3.99 \times 10^4$  receiver gain, 4096 points, employing a time constant of 5.12 ms and conversion time of 10.24 ms resulting in a sweep time of 41.94 s for 10 scans. The red dashed line indicates the simulated spectra, used to calculate the rotational correlation times ( $\tau_R$ ) of the paramagnetic Cu(II) complex

condition) are vastly inferior to those reported using our first-generation cavity [17]; this is solely due to the detuning of the EPR mode owing to the microwave loading effect of the heating port. This noise is, however, suppressed by attaching a coaxial DC to 7.2 GHz low-pass filter to the heating port, thus maintaining the critical coupling of the EPR mode and the signal-to-noise ratio (SNR) of the EPR spectra. This is evident in the improved SNR of the EPR spectra acquired with the low-pass filter in place, as shown in Fig. 6c, d.

As a result of the improved SNR with the addition of the filter, an accurate rotational correlation time ( $\tau_R$ ) could be extracted via full spectral simulation utilising the spin Hamiltonian parameters ( $\mathbf{g}$  and  $\mathbf{A}$ -values expanded on later). From Fig. 6c, and d, a clear decrease in  $\tau_R$  is again, like in our previous work [17], proof that dielectric heating has occurred indicative of faster tumbling of the  $\text{Cu}(\text{acac})_2$  molecules in solution.

The loading effect of the heating port on the coupling of the EPR mode can be experimentally demonstrated by measuring the voltage reflection coefficient  $S_{11}$  of the 9.5 GHz EPR mode with a Keysight E5071C vector network analyser. The EPR mode was first critically coupled by adjusting the depth and orientation of its coupling loop, first with no physical connection to the 6.1 GHz heating port, after which the amplifier circuit was connected, and the measurement repeated. The reduction in coupling strength is clear from Fig. 7a, also giving rise to an input impedance mismatch, both of which are responsible for degrading the EPR spectra. However, if the EPR mode is first critically coupled and the amplifier circuit connected via the low-pass filter, the  $S_{11}$  traces of Fig. 7b are obtained, which show no discernible differences, and so the critical coupling of the EPR mode is retained. The effectiveness of the low-pass filter has already been noted in the high quality EPR spectra presented earlier in Fig. 6c, d.

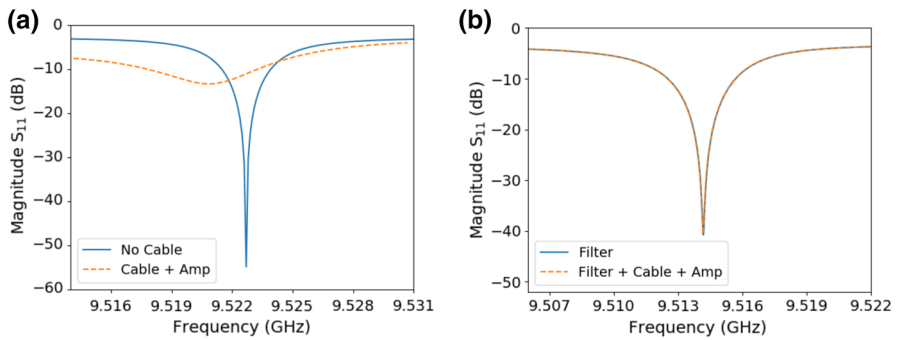


**Fig. 7**  $S_{11}$  measurements of the 9.5 GHz EPR mode on the second-generation dual-mode cavity **a** without the low-pass filter attached to the heating port (left open circuit when cable and amp were not attached), showing the high loading on the EPR mode caused by amplifier circuit, **b** with the DC to 7.2 GHz low-pass filter connected directly to the heating port (left open circuit when filter, cable and amp were not attached), thus resulting in negligible loading effect to the EPR mode, and subsequent improvement in the resulting EPR spectra

The EPR spectra of the  $\text{Cu}(\text{acac})_2$  solution measured with this filter in place are shown in Fig. 6. The SNRs of the CW-EPR spectra recorded with the 1.6 mm tube at 298 K (Fig. 6c) and 318 K (Fig. 6d) were considerably improved by factors of 10 and 5, respectively, in comparison to the data sets recorded in the absence of the 7.2 GHz filter (see Table 1).

Since the inclusion of the low-pass filter was shown to solve the extraneous noise problem when employing a 1.6 mm sample tube, the same procedure was repeated using the more commonly used 4 mm sample tube to maximise the available sample volume; indeed, this requirement to use the more standard 4 mm larger sample tube was one of the primary motivations for changing the coupling position for the heating mode in the first instance. To allow for a direct comparison between spectra obtained with the different tube diameters, and again ensuring maximum cavity filling factor, a 300  $\mu\text{l}$  aliquot of 6.6 mM  $\text{Cu}(\text{acac})_2$  in a  $\text{CHCl}_3$  solution was loaded into the commercially available 4 mm tube (product number: 707-SQ-250 M Wilmad Labglass, O.D.=4 mm and I.D.=3 mm), such that the total number of spins

**Table 1** SNR and double integration (D.I) of the  $\text{Cu}(\text{acac})_2$   $\text{CHCl}_3$  solutions recorded in the presence and absence of the 7.2 GHz low-pass filter on the heating port

Temperature (K)	Tube size (mm)	SNR	D.I
298			
No filter	1.6	9.8	-
Filter	1.6	99.1	$4.3 \times 10^5$
Filter	4.0	114.9	$4.8 \times 10^5$
318			
No filter	1.6	4.3	-
Filter	1.6	23.2	$3.2 \times 10^5$
Filter	4.0	35.2	$3.6 \times 10^5$

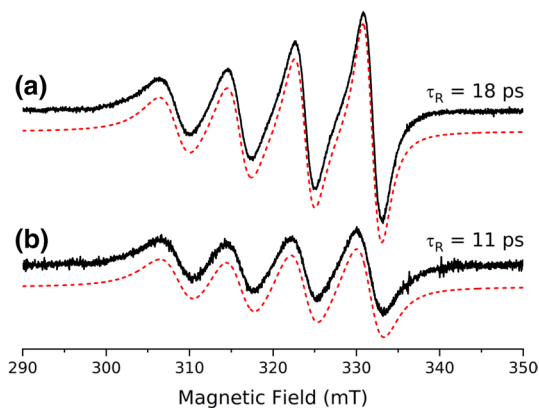
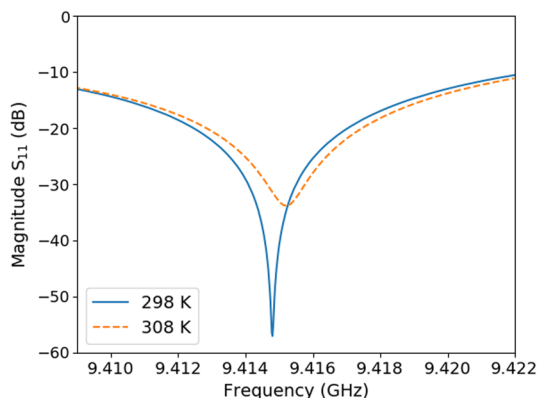


**Fig. 8** X-band CW-EPR spectra of 6.6 mM  $\text{Cu}(\text{acac})_2$  in  $\text{CHCl}_3$  recorded in a 4 mm tube with the 7.2 GHz low-pass filter at **a** 298 K and **b** 318 K. Both spectra were acquired on the second-generation composite Cu/Al dual-mode cavity, employing 100 kHz field modulation, 0.1 mT modulation depth,  $3.99 \times 10^4$  receiver gain, 4096 points, employing a time constant of 5.12 ms and conversion time of 10.24 ms resulting in a sweep time of 41.94 s for 10 scans. Red dashed lines indicate simulated spectra from which rotational correlation times ( $\tau_R$ ) were determined

in the sampled solution was identical to that previously used with the 1.6 mm tube (20 mM, 100  $\mu\text{l}$ ). The resulting EPR spectra are shown in Fig. 8, yielding SNR and double integral values in an acceptable range, compared to the sample recorded in the smaller tube (see Table 1). One may have expected an increase in sensitivity with increased sample tube diameter (4 mm). This is not seen in Table 1 through evaluation of the SNR and D.I., likely due to the 4 mm tube having a higher degree of encroachment into the EPR E field, reducing  $Q$  factor and hence sensitivity resulting in these values to be lower at both 298 K and 318 K compared to the 1.6 mm tube. These experiments demonstrate that microwave heating can successfully be achieved with larger tube diameters, which will be important for future studies of low concentration samples for which maximum sample volume is desired.

To conclude this experimental EPR section, we note the effect of increased temperature on the coupling coefficient of the EPR mode. For samples that are mixed with or dissolved in polar solvents, the dielectric loss of the host solvent will decrease on increasing the temperature owing to an increase in the Debye frequency [22], which will also cause a reduction in their relative permittivity. Although samples are placed in a node of electric field in an EPR cavity, the mode is a mathematical line so any finite sample size will lead to the sample being exposed to a small electric field. The reduced dielectric loss with increasing temperature will then lead to an increase in the  $Q$  of the EPR mode, so that any critical coupling condition (coupling coefficient  $g = 1$ ) set experimentally at room temperature will give way to overcoupling ( $g > 1$ , since  $g \propto Q$ ) as the temperature rises; this will reduce the EPR signal. To demonstrate this effect, the  $S_{11}$  values of the cavity containing a 1.6 mm tube filled with  $\text{CHCl}_3$  were recorded at 298 K and 308 K. The frequency increases owing to the reduction in the relative permittivity  $\epsilon_1$  of  $\text{CHCl}_3$  as the temperature increases, which results in the detuning of the

**Fig. 9**  $S_{11}$  measurements of the EPR mode when loaded with a 1.6 mm quartz tube filled with  $\text{CHCl}_3$ , at temperatures of 298 and 308 K. As temperature increases, the permittivity and microwave loss of the solvent decrease, causing a small increase in resonant frequency and increase in  $Q$ , resulting in the EPR mode becoming overcoupled



cavity, and the insertion loss at resonance is less negative (from  $-57$  to  $-33$  dB). The results are shown in Fig. 9 and, although the changes are small, since the EPR mode has such a high  $Q$  ( $>5000$ ) and thus narrow 3 dB bandwidth ( $<2$  MHz) the effects on the resulting EPR signal are large. This observed decrease in coupling strength on increasing temperature is the most likely cause of the decrease in resulting EPR signal intensity at 318 K (Figs. 6d and 8b), as monitored by the double integrals (D.I) of the EPR signal (Table 1). Ongoing design alterations will enable the cavity to be recoupled (i.e., “re-tuned”) safely at higher temperatures, thus preserving the EPR signal strength.

Finally, we present a further analysis of the EPR spectra shown in Figs. 6 and 8. As stated previously, simulations of the experimental isotropic EPR spectra enable to determine the characteristic time associated with rotational diffusion (i.e., molecular tumbling) in solution, namely, rotational correlation time,  $\tau_R$ . Spectra simulation and derivation of the molecular dynamics parameters were carried out solving the stochastic Liouville equation (SLE) using a full matrix diagonalization approach and fitting the simulated spectra to a model of isotropic rotational diffusion implementing a Nelder/Mead downhill simplex method. The magnetic  $\mathbf{g}$  and  $^{\text{Cu}}\mathbf{A}$  tensors used for the simulation were  $\mathbf{g}=[2.037\ 2.037\ 2.279]$  and  $^{\text{Cu}}\mathbf{A}=[-45\ -45\ -585]$  MHz, in close agreement with the values reported by Ritterskamp et al. [23]. The entire spectra simulation/fitting work was carried out using EasySpin, an open-source MATLAB toolbox for simulating and fitting a wide range of Electron Paramagnetic Resonance spectra [24]. At 298 K and 318 K, the values of  $\tau_R$  were found to be ca. 18 ps and 9–11 ps, respectively, in good agreement with the estimates obtained using our first-generation dual-mode cavity [17].

Once again, the decrease in  $\tau_R$  upon application of the 6.1 GHz mode is a clear indication that in situ heating has been successful, as shown by faster rotational diffusion of the complex in solution. Faster rotational diffusion can be explained through the dipolar rotation mechanism of dielectric heating, causing solvent molecules and consequently  $\text{Cu}(\text{acac})_2$  molecules to rotate faster at higher temperatures, leading to an increase in motional isotropy detected by CW-EPR, i.e., a clear way of assessing the cavity’s effectiveness of heating.

## 4 Conclusion

We have presented several design improvements to a dual-mode EPR cavity that enables effective and simultaneous microwave heating during EPR detection. The key improved design principles include the replacement of the aluminium cavity walls with commercial copper laminates, permitting a satisfactory penetration of the modulation field into the cavity's sample space. Reorientation of the 6.1 GHz heating coupling port to a 135° positioning with respect to the 9.5 GHz EPR port crucially facilitates the use of larger sample volumes. Finally, attachment of a 7.2 GHz low-pass filter to the heating port is crucial for reducing extraneous noise. Further work is currently underway to improve the coupling of the cavity upon application of the 6.1 GHz. The experimental EPR spectra presented here illustrate the efficiency of employing *in situ* microwave heating to directly study molecular motions in solution, and we will present additional enhancements in future contributions, including the ability to adjust the coupling of the EPR mode at higher temperatures and enable more rapid temperature jumps in the sampling system, of relevance to kinetic measurements in catalytic reactions. Conventional heating methods do not allow for real time analysis of paramagnetic chemical systems. Due to the instantaneous nature of microwaves, this functionality should be possible using the methods presented in this work, which is lacking using conventional heating methods utilised currently in EPR.

**Acknowledgements** EPSRC funding (EP/R04483X) is gratefully acknowledged. Dr Heungjae Choi was funded by the EPSRC Programme Grant GaN-DaME (EP/P00945X/1) and was funded by the Sêr Cymru II Fellowship by the European Regional Development Fund through the Welsh government (TG/KJB/VSM:1103515). Information on the data underpinning the results presented here, including how to access them, can be found in the Cardiff University data catalogue at <https://doi.org/10.17035/d.2021.0139141355>.

**Open Access** This article is licensed under a Creative Commons Attribution 4.0 International License, which permits use, sharing, adaptation, distribution and reproduction in any medium or format, as long as you give appropriate credit to the original author(s) and the source, provide a link to the Creative Commons licence, and indicate if changes were made. The images or other third party material in this article are included in the article's Creative Commons licence, unless indicated otherwise in a credit line to the material. If material is not included in the article's Creative Commons licence and your intended use is not permitted by statutory regulation or exceeds the permitted use, you will need to obtain permission directly from the copyright holder. To view a copy of this licence, visit <http://creativecommons.org/licenses/by/4.0/>.

## References

1. V. Chechik, E. Carter, D.M. Murphy, *Electron Paramagnetic Resonance* (Oxford University Press, Oxford Chemistry Primers, 2016)
2. M.R. Dent et al., Electron paramagnetic resonance spectroscopy as a probe of hydrogen bonding in heme-thiolate proteins. *Inorg. Chem.* **58**(23), 16011–16027 (2019)
3. D. Hinderberger, H.W. Spiess, G. Jeschke, Dynamics, site binding, and distribution of counterions in polyelectrolyte solutions studied by electron paramagnetic resonance spectroscopy. *J. Phys. Chem. B* **108**(12), 3698–3704 (2004)
4. A. Dasgupta, E. Richards, R.L. Melen, Frustrated radical pairs: insights from EPR spectroscopy. *Angew. Chemie* **133**(1), 53–65 (2021)

5. G. Rao et al., Metal bonding with 3d and 6d orbitals: an EPR and ENDOR spectroscopic investigation of  $Ti^{3+}$ -Al and  $Th^{3+}$ -Al heterobimetallic complexes. *Inorg. Chem.* **58**(12), 7978–7988 (2019)
6. E. Morra, E. Giamello, M. Chiesa, EPR approaches to heterogeneous catalysis. The chemistry of titanium in heterogeneous catalysts and photocatalysts. *J. Magn. Reson.* **280**, 89–102 (2017)
7. M. Goswami, A. Chirila, C. Rebreyend, B. de Bruin, EPR spectroscopy as a tool in homogeneous catalysis research. *Top. Catal.* **58**(12–13), 719–750 (2015)
8. S. Van Doorslaer, D.M. Murphy, EPR spectroscopy in catalysis. *EPR Spectroscop.: Appl. Chem. Biol.* (2012).
9. J. Spencer, A. Folli, E. Richards, D. M. Murphy, Applications of electron paramagnetic resonance spectroscopy for interrogating catalytic systems. in *Specialist Periodical Reports*, ed. by V. Chechik, D.M. Murphy, vol 26, (RSC (Royal Society of Chemistry), 2019). Series ISSN: 1464-4622. ISBN: 978-1-78801-372-7
10. S. Tussing, J. Paradies, Microwave-assisted FLP-catalyzed hydrogenations. *Dalt. Trans.* **45**(14), 6124–6128 (2016)
11. J.L. Carden, L.J. Gierlich, D.F. Wass, D.L. Browne, R.L. Melen, Unlocking the catalytic potential of tris(3,4,5-trifluorophenyl)borane with microwave irradiation. *Chem. Commun.* **55**(3), 318–321 (2019)
12. H. Li, C. Zhang, C. Pang, X. Li, X. Gao, The advances in the special microwave effects of the heterogeneous catalytic reactions. *Front. Chem.* **8**(355), 1–8 (2020)
13. A. Kokel, C. Schäfer, B. Török, Application of microwave-assisted heterogeneous catalysis in sustainable synthesis design. *Green Chem.* **19**(16), 3729–3751 (2017)
14. D. Stuerge, K. Gonon, M. Lallemand, Microwave heating as a new way to induce selectivity between competitive reactions. Application to isomeric ratio control in sulfonation of naphthalene. *Tetrahedron* **49**(28), 6229–6234 (1993)
15. J.E. Crooks, The temperature-jump technique for the study of fast reactions in solution. *J. Phys. E.* **16**(12), 1142–1147 (1983)
16. A. Marchand, M.F. Czar, E.N. Eggel, J. Kaeslin, R. Zenobi, Studying biomolecular folding and binding using temperature-jump mass spectrometry. *Nat. Commun.* **11**(1), 566 (2020)
17. A. Folli et al., A novel dual mode X-band EPR resonator for rapid in situ microwave heating. *J. Magn. Reson.* **310**, 106644 (2020)
18. J.S. Hyde, J.W. Sidabras, R.R. Mett, Uniform field resonators for EPR spectroscopy: a review. *Cell Biochem. Biophys.* **77**(1), 3–14 (2019)
19. S.Z. Kiss et al., A microwave resonator integrated on a polymer microfluidic chip. *J. Magn. Reson.* **270**, 169–175 (2016)
20. G.R. Eaton, S.S. Eaton, D.P. Barr, R.T. Weber, “*Basics of Continuous Wave EPR*”, in *Quantitative EPR* (Springer Vienna, Vienna, 2010), pp. 1–14
21. S. Pisa et al., Design and Realization of an Open EPR Resonator at X-Band Frequencies. *IEEE Trans. Magn.* **55**(2), 1–10 (2019)
22. U. Kaatze, Complex permittivity of water as a function of frequency and temperature. *J. Chem. Eng. Data* **34**(4), 371–374 (1989)
23. N. Ritterskamp et al., Understanding the Coordination Modes of  $[Cu(acac)_2]$  (imidazole)  $n = 1,2$  Adducts by EPR, ENDOR, HYSCORE, and DFT analysis. *Inorg. Chem.* **56**(19), 11862–11875 (2017)
24. S. Stoll, A. Schweiger, EasySpin, a comprehensive software package for spectral simulation and analysis in EPR. *J. Magn. Reson.* **178**(1), 42–55 (2006)

**Publisher's Note** Springer Nature remains neutral with regard to jurisdictional claims in published maps and institutional affiliations.